How magmatic storage regions attract and repel propagating dikes

Pansino, Stephen; Taisne, Benoit

2018

Pansino, S., & Taisne, B. (2019). How magmatic storage regions attract and repel propagating dikes. Journal of Geophysical Research: Solid Earth, 124(1), 274-290. doi:10.1029/2018JB016311

https://hdl.handle.net/10356/89854

https://doi.org/10.1029/2018JB016311

JGR Solid Earth

RESEARCH ARTICLE
10.1029/2018JB016311

How Magmatic Storage Regions Attract and Repel Propagating Dikes

Stephen Pansino[1] and **Benoit Taisne**[1,2]

[1]Earth Observatory of Singapore, Nanyang Technological University, Singapore, Singapore, [2]Asian School of the Environment, Nanyang Technological University, Singapore, Singapore

Key Points:
- Dike propagation is generally attracted to overpressure magma reservoirs and repelled by underpressure reservoirs
- The mechanism that attracts or repels dikes differs, depending on the dike's initial orientation
- The likelihood of satellite/off-axes eruptions increases following large eruptions and evolves with time following viscous stress relaxation

Supporting Information:
- Supporting Information S1
- Movie S1
- Movie S2
- Movie S3
- Movie S4

Correspondence to:
S. Pansino,
steve.pansino@gmail.com

Citation:
Pansino, S., & Taisne, B. (2019). How magmatic storage regions attract and repel propagating dikes. *Journal of Geophysical Research: Solid Earth*, *124*, 274–290. https://doi.org/10.1029/2018JB016311

Received 2 JUL 2018
Accepted 17 DEC 2018
Accepted article online 20 DEC 2018
Published online 19 JAN 2019

Abstract We investigate the effect of magmatic reservoir pressure on the propagation of dikes that approach from below, using analogue experiments. We injected oil into gelatin and observed how dike propagation responded to the stress field around a pressurized, spherical reservoir, filled with water. The reservoir was modeled using two different setups: one simply using an inflatable rubber balloon and the other by constructing a liquid-filled cavity. We find that the dike's response is dependent on the sign of the reservoir pressure (i.e., inflated/overpressurized and deflated/underpressurized) as well as on the dike's initial orientation (i.e., if its strike is radially, circumferentially, or obliquely oriented to the reservoir). Dikes that are initially strike radial respond, respectively, by propagating toward or away from overpressurized or underpressurized reservoirs, taking advantage of the reservoir's hoop stresses. Otherwise-oriented dikes respond by changing orientation, twisting and curling into a form dictated by the principal stresses in the medium. For overpressurized reservoirs, they are coaxed to propagate radially to, and therefore approach, the reservoir. For underpressurized reservoirs, they generally reorient to propagate tangentially, which causes them to avoid the reservoir. The magnitude of reservoir pressure controls at which distance dikes can be affected, and, at natural scales, we estimate that this occurs within a radius of a few tens of kilometers. This diminishes with time, due to viscous stress relaxation of the crust, which will occur on a timescale of hundreds of years.

Plain Language Summary Magma commonly moves up toward the surface by creating cracks in the crust. It flows inside of the cracks and propagates by applying pressure that drives the flow and damages surrounding rocks. Nature always finds the easiest path for the crack, so if it takes less pressure to push apart the ground vertically or horizontally, the crack will grow accordingly. As it makes its way to the surface, it may encounter local stress variations that change its propagating direction. This applies near magma storage regions, below volcanoes. If such a region is highly pressurized or deflated, then nearby cracks will "feel" the change in their surrounding conditions and react by aligning in a direction of favorable stress. This makes it look like they are growing toward or circling around the storage region, respectively. We studied this behavior using scaled model experiments in laboratory conditions. We use different types of materials to represent nature, such as gelatin as rock and oil as magma. We were able to show how these cracks change shape for different reservoir pressures. We found that after a large eruption, subsequent eruptions are more likely to occur farther from the summit of a volcano.

1. Introduction

When magma ascends from depth toward a shallow magmatic storage region, it can either migrate via an existing pathway (i.e., a conduit) or fracture open a new pathway in the form of a dike. Deeply sourced feeder dikes can supply large volumes of mafic magma, which may either arrive to a shallower reservoir and mingle with the existing magma or bypass the reservoir and erupt at the surface. For example, some monogenetic eruptions at Sanganguey volcano (Mexico) emit lavas that come directly from a deep reservoir, while others emit lavas that represent a mixture of deeply and shallowly residing magmas (Crabtree & Waters, 2017). The path that a feeder dike takes depends on the state of stresses in the crust, and one significant source of stress can be a pressurized magmatic reservoir, which has been shown can attract feeder dikes (Karlstrom et al., 2009). Generally speaking, when fresh magma arrives to a magmatic storage region, it is thought to remobilize the residing magma, which can lead to an eruption (Murphy et al., 2000; Ruth et al., 2016). Whether a dike propagates toward a shallow reservoir and mingles with the shallow magma, or bypasses the reservoir, has an effect on the probability, location, and style of eruption, which has important

implications for hazards and risk management. We therefore want to understand how dikes propagate in the presence of a pressurized or underpressurized magmatic reservoir.

Dikes are known to be oriented according to the stresses in the crust and open against the least compressive principal stress, σ_3, and propagate perpendicular to this direction (Delaney, 1986). If a dike enters a localized stress field, such as that due to a pressurized magma storage region, it can twist and curl into its preferred orientation. For example, Porreca et al. (2006) show that dikes in the Mt. Somma scarp near Vesuvius take a range of orientations, from radial to circumferential, from inward to outward dipping, and posit that this is due to varying reservoir pressures at the time of emplacement. This is because a pressurized reservoir favors radial emplacement, while a depressurized one favors tangential orientation (Bianco et al., 1998). Indeed, at the well-exposed Ardnamurchan dike swarm, Anderson (1937) interprets inward dipping circumferential dikes as sourced from an overpressurized reservoir and outward-dipping dikes sourced from an underpressurized reservoir. More recently at the same location, Magee et al. (2012) show via the anisotropy of magnetic susceptibility that magma flow was dominantly horizontal and that the flow aligned similarly to nearby NW-SE trending regional dikes. They proposed that the circumferential and regional dikes are linked and that the local circumferential pattern was due to the reservoir's pressure.

The competition between local and regional stress fields can be evident from a dike's orientation. On the volcanoes of the Galapagos Islands, for example, swarms of dikes tend to align either circumferentially near the edifices or radially a bit further away (Chadwick & Dieterich, 1995). This is because many of the volcanoes have calderas, whose formation causes unloading of the underlying crust. This generates an extensional force that causes dikes, originating from the reservoir, to emplace in such orientations (Bagnardi et al., 2013). This also would cause any subsequent feeder dikes, ascending from below, to deflect laterally away and eventually erupt at the caldera rim (Chadwick & Dieterich, 1995; Corbi et al., 2016). Away from the collapse structure, the stress field is configured differently, and dikes take on a radial pattern. For another example, using geophysical monitoring techniques, Gudmundsson et al. (2014) show that during the 2014 Bárðarbunga eruption (Iceland), a dike intruded into the crust from a pressurized reservoir and began to propagate radially away. Some kilometers away, the dike rotated by ~30° to match the orientation of the regional stresses.

Dikes can also change orientation due to other factors. Crustal heterogeneities (e.g., layers) play a significant role, deflecting dikes into sills, in that a strong overlying layer may cause dike propagation to come to arrest (Rivalta et al., 2005). If the two layers are not strongly coupled together, pressure accumulation at the interface may lead to failure and decoupling, allowing the magma to form a sill (Kavanagh et al., 2015). Furthermore, a propagating dike or sill can abruptly change orientation at its leading edge, due to the balance of internal forces and the cohesive strength of the surrounding crust (Galland et al., 2014; Schmiedel et al., 2017). Galland et al. (2014) show using analogue experiments with silica powder that if a dike or sill is shallow (overlying compressional forces are low) and has a high viscosity and/or high influx rate (internal pressure is high), it can divert into a cone sheet.

The direction in which a dike propagates depends on the orientation of the principal stresses in the crust, as well on the distribution of stresses (i.e., if there is a vertical or horizontal gradient in magnitude). Watanabe et al. (2002) shows with analogue experiments, injecting silicon oil into gelatin, that a surface load reorients the stress field to attract dikes. Maccaferri et al. (2011) show similar results numerically, by modeling a boundary element liquid-filled crack, for various loadings and dike angles of ascent. In both cases, the strike of the dike is oriented circumferentially to the loading, and the dike curls inward toward the edifice load. An edifice's load, however, can induce a compressive state on the underlying crust and inhibit dike propagation (Pinel & Jaupart, 2003). Dikes that propagate into such a region may either come to arrest or begin horizontal propagation at their lateral edges. Urbani et al. (2018) use analogue modeling to extend this concept to topography more generally and show that dikes propagate away from topographic highs to erupt in topographic lows.

It is clear that dikes respond to stresses in the crust in a complex fashion and that their ability to interact with existing magma bodies has important hazards implications, such as influencing the location of future eruptions. We therefore investigate how dikes respond (i.e., how they bend and change orientation or how they propagate horizontally) to a pressurized (i.e., inflated or deflated) magmatic reservoir using analogue experiments. This allows us to explore such responses simply by varying the initial conditions, which are the initial

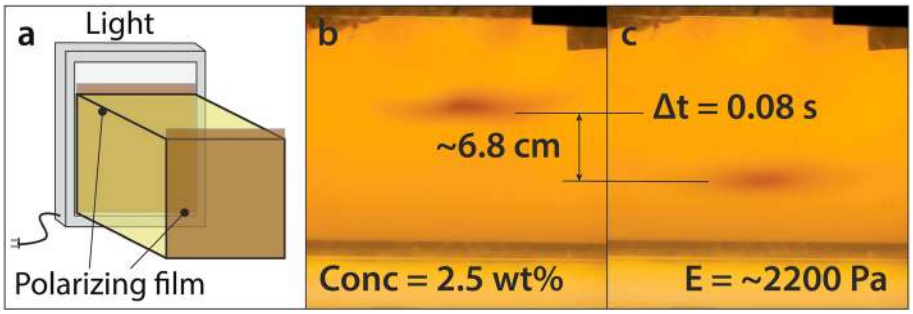

Figure 1. (a) A drawing of the setup to visualize shear waves. Light passes through polarizing filters, placed in front of and behind the experimental tank. Stresses perturbation within the gelatin become visible, and, by gently exciting the gelatin surface, we can see shear waves propagating. (b and c) Two sequential images of a shear wave (dark region) propagating downward through a solid gelatin. The velocity is used to estimate the gelatin's Young's modulus.

dike orientation and the magnitude of reservoir inflation or deflation. For a small subset of experiments, we use a different setup to secondarily investigate how dikes behave when they intersect with the reservoir. These simple models can be intuitive and descriptive and allow us to simulate complex three-dimensional behavior that cannot readily be modeled via numerical methods.

2. Methods

Throughout this study we refer to dikes in different orientations, relative to the reservoir (Figure S4, in the supporting information). The following terminology will be adopted:

1. *Radial* or *strike radial*: We use in the conventional sense to indicate dikes that are vertically oriented and whose strikes are radial to the reservoir.
2. *Circumferential* or *strike circumferential*: We generally use this in the conventional sense as well, for dikes whose strikes are oriented tangential to the map-view projection of the reservoir. Such dikes can propagate radially to the reservoir, in the way that a cone sheet does, but are not "radial dikes." We use this for both inward and outward dipping dikes.
3. *Oblique*: Dikes whose strikes are initially oblique (45°) to the map-view projection of the reservoir.
4. *Coaxial*: Dikes whose vertical leading tips are aligned with the center of the map-view projection of the reservoir. They are positioned directly below the reservoir.
5. *Nonradial*: We use this to mean dikes in our experiments that were not radial dikes, meaning circumferential, oblique, and coaxial dikes.

2.1. Experimental Procedures

We performed the experiments in 40 × 40 × 30 cm (length, width, and height) and 50 × 50 × 50 cm tanks, filled with 3.75 wt% industrial gelatin (250 bloom). The retailer did not specify the animal source beyond beef or pork (see the supporting information), though the two sources have been shown to be mechanically similar (Nur Hanani et al., 2012). We prepared each gelatin in a similar way, by mixing gelatin granules into a pot of purified water and slowly heating the pot to 60 °C, while constantly stirring with an overhead stirrer (Di Giuseppe et al., 2009; Tosh et al., 2003). We added a small splash of bleach to the gelatin to mitigate bacteria growth, which causes the gelatin to become cloudy in appearance. The resulting liquid gelatin is then placed in our cold room (15 °C) to solidify for 72 hr, with a layer of oil on the surface to prevent evaporation.

Gelatin is an ideal medium for such experiments, as it can scale to the Earth's crust and is transparent, so we can observe what occurs inside (Di Giuseppe et al., 2009; Galland et al., 2015; Kavanagh et al., 2013; Rivalta et al., 2015). Due to the slight variations in the preparation (initial temperature, cooling time, and cooking time/evaporation), it varies somewhat in strength from experiment to experiment, which we measure. Gelatin is a photoelastic material, so we can measure the gelatin's strength at the beginning of each experiment via the velocities of shear waves, which become visible using a pair of polarizing filters (Figure 1; Taisne & Tait, 2011). When light passes through these filters, it becomes linearly polarized to a particular incidence angle. As light passes through the gelatin, its retardation depends on the stress level and the

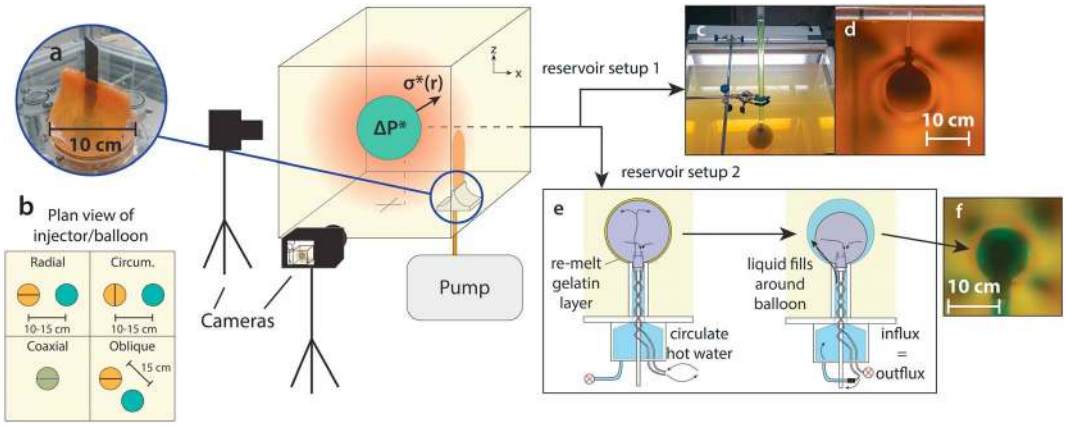

Figure 2. Schematic of our experimental setup. A balloon embedded in gelatin is pressurized and a pump injects oil. We record the experiments with cameras from different perspectives. (a) Our dike injection piece, shown attached to the bottom of an empty tank. It contains a sliding blade that makes an initial cut in the gelatin, into which oil is pumped. (b) Plan view showing the balloon and injector positioning and offset, for different dike orientations. The injector location is somewhat constrained and can be rotated in 90° increments, so we move the balloon to control distance and orientation. (c) An embedded balloon in a gelatin is pressurized or depressurized via a vertical tube (here we show experiment 5; see Table 1 for experimental conditions). (d) The corresponding deviatoric stress field shown using polarized filters. The repeating rainbow pattern indicates the stress gradient and allows us to minimize boundary effects. (e) An apparatus allows us to construct a liquid reservoir without a balloon. Hot water is circulated into a balloon to remelt a layer of surrounding gelatin. The balloon is deflated and surrounded with dyed water. (f) A photo showing the final cavity in a pressurized state (experiment 1).

light's wavelength (Ramesh, 2000). This enables us the see the deviatoric stress in the gelatin and is sensible enough to visualize propagating stress perturbation generated at the surface. The shear modulus of the gelatin, G, is directly proportional to the shear wave velocity, v_s, via

$$G = \rho v_s^2, \tag{1}$$

where ρ is the gelatin's density (Lee et al., 2017). For a weak material like gelatin, these shear waves can be quite slow (~1 m/s) and are easy to track with a simple camera or the unaided eye. Finally, the Young's modulus, E, can be found via

$$E = 2G(1 + \nu), \tag{2}$$

where ν is the Poisson's ratio of the medium.

We injected dikes from the base of the tank using an injection piece attached to a pump, which we used to supply the liquid. The piece contains a retractable blade inside, which forms an initial precut (Figure 2a), forcing the dikes into our preferred, vertical orientation. We set the balloon and injector position so that the dike's initial strike is oriented either radial (experiments 1 and 2), circumferential (experiments 3 and 4), oblique at a 45° angle (experiments 5 and 6), or coaxial (experiment 7) to the reservoir (Figure 2b). For the injected liquid, we used vegetable oil mixed with chili powder (to provide pigment), which is less dense than gelatin and rises buoyantly. We generally injected constant volume dikes, in that we pumped in the oil with a moderately fast influx over a period of a few minutes, turned off the pump, and allowed the dikes to ascend solely due to their buoyancy. Dikes extended in length, and the tail region remained filled with the initial liquid. For two experiments, we had constant-flux conditions, in that we never stopped injecting oil, so the dike propagated primarily due to the driving pressure (from the pump) and less due to buoyancy.

To model the reservoir, we used two different setups, both of which achieved the primary goal of generating a stress field around the reservoir. For the first setup we embedded, from above, a simple latex balloon in the gelatin (while still warm and liquid), with a diameter of ~10 cm and with its center positioned ~15 cm below the surface. We accessed the balloon using a vertical tube (Figure 2c), which we filled with water to apply hydrostatic pressure to the balloon and thereby maintain its diameter. After the gelatin solidified, the balloon could be further inflated or deflated (via the tube) to apply a compressive or extensional deviatoric stress to the system (Figure 2d). With this setup, the balloon acts as a physical barrier, so we could not observe interchange of liquids between the dike and reservoir, but we could model the stress field around the

reservoir. We used polarized film to visualize the extent of the stress distribution and minimize their interaction with the tank walls, thereby mitigating boundary effects. Stress visualization helped us ensure that we injected the dikes into a region of low stress, which allowed us to observe their behavior as they entered the stress field around the balloon. For the second setup, we wanted to be able to assess the fluid exchange between the reservoir and dike, and so we designed a specific apparatus to construct a balloon-less reservoir. This piece allowed us to embed a pressurized balloon in the gelatin, then deflate it and replace it with dyed water (Figure 2e). The liquid-filled cavity could then be further pressurized to perform the experiment (Figure 2f). The setup is a bit complicated, and so we explain it further in the supporting information.

We recorded the experiments using typical cameras, which took a time lapse of photographs from different perspectives and allowed us to track the dikes' position and geometry (see Pansino & Taisne, 2018, for data repository). We took photos in 18-MP resolution at a frequency of 6 photos per minute, which was high relative to the dike velocity (generally <1 mm of propagation between photos).

2.2. Scaling

The scaling and analysis of this study rely on the deviatoric stresses in the medium, in which the magnitude at any radial distance from the center of reservoir, r, is a function of the reservoir's internal pressure and radius, respectively, ΔP and r_{res}. This has components that are radial and tangential to the reservoir, respectively, denoted as σ_{rr} and σ_{tt}:

$$\sigma_{rr}(r) = \Delta P\,(r_{res}/r)^3 \tag{3}$$

and

$$\sigma_{tt}(r) = -(1/2)\,\Delta P\,(r_{res}/r)^3. \tag{4}$$

This assumes the medium behaves as an infinitely-thick-walled, spherical pressure vessel (Segall, 2010). A pressurized reservoir exerts compressive forces on the medium in the radial direction but places it in a state of extension in the tangential direction. A negative pressure contracts the medium, causing the reverse effect. The minimum compressive stress, σ_3, which a dike opens against, is the lesser of these two components, so a nearby dike's preferred orientation (radial or tangential) depends on the sign of the reservoir pressure. The hoop stress (i.e., the σ_{tt} component) can have a secondary effect on radially oriented dikes, either helping or hindering propagation along the nearest edge of the dike.

For comparison with natural systems, we scale the stress distribution against the fracture pressure of the dike, P_f, which quantifies the amount of pressure necessary for a dike to fracture the medium, and therefore propagate

$$\sigma^* = |\sigma_3|/P_f. \tag{5}$$

The dimensionless stress, σ*, essentially maintains that the magnitude of stress is proportional to the strength of the material. This is a similar approach as taken by Daniels and Menand (2015), who scale regional extensional stresses against dike buoyancy forces; we will also incorporate buoyancy into the scaling. Following Lister and Kerr (1991),

$$P_f = K_c/{L_b}^{1/2}, \tag{6}$$

Menand and Tait (2002),

$$K_c = (2\gamma E)^{1/2}, \tag{7}$$

and Taisne and Tait (2009),

$$L_b = (K_c/\Delta\rho g)^{2/3}. \tag{8}$$

L_b is the buoyancy length, the minimum length a dike must surpass to buoyantly rise through the crust without any external driving pressure. K_c and γ are, respectively, the fracture toughness and surface energy of the

Table 1
Experimental Conditions

Parameter (units)	Exp 1	Exp 2	Exp 3	Exp 4	Exp 5	Exp 6	Exp 7
E (Pa)	4,642	2,750	5,272	3,424	3,311	3,719	3,827
Gelatin volume (L)	112	100	48	112	100	100	100
Cold room temperature (°C)	15	15	15	15	15	15	15
Cooling time (days)	5	3	3	4	3	3	4
Dike initial orientation	Radial	Radial	Circum.	Circum.	Oblique	Oblique	Coaxial
$\Delta\rho$ (kg/m^3)	100	100	100	100	100	100	100
Reservoir diameter (cm)	9.9	8.3	10.1	7.6	10.7	7.9	8.6
Reservoir depth (cm)	16.6	8.6	8.8	16.7	14.9	14.3	13.1
Dike—reservoir horizontal offset (cm)	16.3	10.3	11.0	16.1	14.1	14.1	0.0
P_f (Pa)	209	175	218	189	187	194	196
Injection type[a]	CV	CV	CF[b]	CV	CV	CV	CF
Volume or rate (ml, ml/min)	120	50	4.25	100	72	144	20
Overpressured/underpressured	Over	Under	Over	Under	Over	Under	Under
ΔP (Pa)	124	−378	1,079	−96	325	−545	−356
ΔP*	0.6	−2.2	5.0	−0.5	1.7	−2.8	−1.8

Note. E = Young's modulus; $\Delta\rho$ = gelatin-dike density contrast; P_f = gelatin fracture pressure; ΔP = reservoir pressure; ΔP* = dimensionless reservoir pressure. [a]Constant volume (CV) or constant flux (CF). [b]At this moment, we did not have good control over the driving pressure of the dike. We believe the pressure was fairly constant, but there was likely some fluctuation.

medium (both material properties). $\Delta\rho$ is the fluid-medium density difference, and g is gravity. Equations (6)–(8) can be combined to relate P_f to the medium's strength properties and the dike's buoyancy:

$$P_f = (2\gamma E \Delta\rho g)^{1/3}. \tag{9}$$

In our experiments, we injected vegetable oil (~910 kg/m^3) into gelatins of 3.75 wt% concentration (~1,010 kg/m^3, measured via a sample's mass and volume offset when submerged in water), leading to a $\Delta\rho$ of 100 kg/m^3 for all experiments (Table 1). We assume γ to be 1 J/m^2 (Kavanagh et al., 2013), and E ranges between 3.3 and 5.3 kPa (derived from direct measurement of G). For ΔP, we estimate the reservoir pressure using its change of radius due to inflation or deflation, Δr_{res}. The strain associated to the reservoir expansion or contraction is simply related to the stress at its outer margin via the Young's modulus, assuming small radius variation:

$$\Delta P = E \Delta r_{res} / r_{res}. \tag{10}$$

We label $\sigma^*(r)$ at the reservoir wall margin as ΔP^*:

$$\Delta P^* = \sigma^*(r_{res}) = \Delta P / P_f. \tag{11}$$

Under these conditions, $|\Delta P^*|$ ranges from 10^{-1} to 10. This overlaps with natural systems, which are estimated to have a similar range of 10^0–10^3 at the reservoir boundary, neglecting viscoelastic effects around the reservoir and using values listed in Table 2. The maximum magnitude of σ^* is ΔP^* at the reservoir boundary and approaches 0 at large radii.

Table 2
Comparison of Values Between Experiments and Natural Systems

Symbol (unit)	Meaning	Experiments[a]	Nature
ΔP (Pa)	Reservoir pressure	10^2–10^3	10^5–10^{8b}
E (Pa)	Young's modulus	~2,500–5,500	$10^{10.5}$
$\Delta\rho$ (kg/m^3)	Medium-liquid density difference	100	100[c]
γ (J/m^2)	Surface energy	1[d]	1[d]
ν	Poisson's ratio	0.5	0.25
ΔP*	Dimensionless reservoir pressure	10^{-1}–10^1	10^0–10^3

[a]All values in experiments column were measured in our lab, unless otherwise noted. [b]Karlstrom et al. (2009). [c]Taisne and Tait (2009). [d]Kavanagh et al. (2013).

3. Results

3.1. Qualitative Observations

We note two classifications of dike response, which depend on the dike's initial orientation. Strike-radial dikes propagated vertically at the outset of each experiment and, as they approached the reservoir, began to propagate horizontally as well (Figures 3a and 3b). We believe that the dikes took advantage of the hoop stresses around the reservoir, which encouraged lateral movement. For the overpressurized experiment (experiment

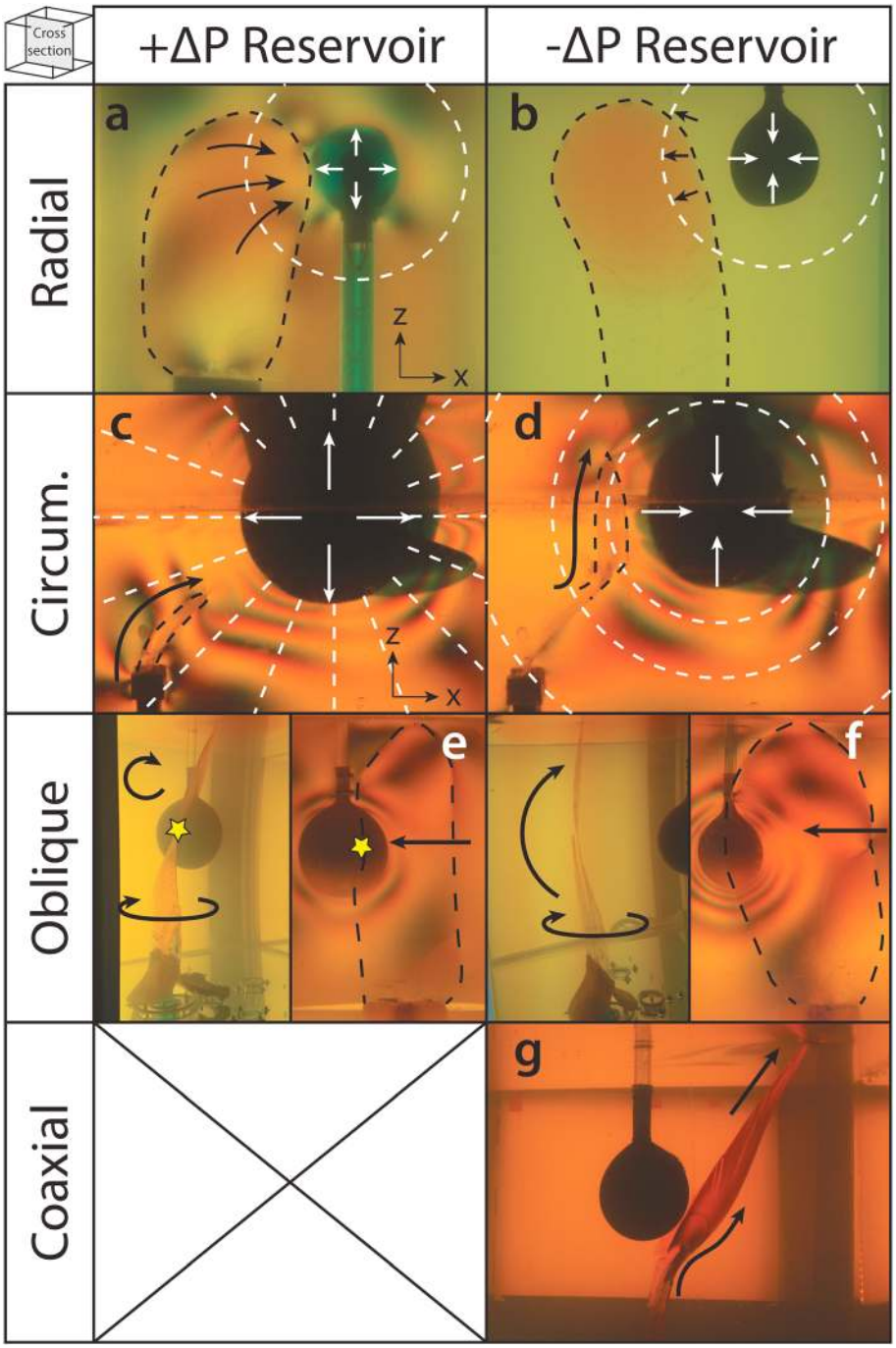

Figure 3. Annotated photos (all in cross-sectional view) depicting different dike responses, depending in the initial dike orientation (each row) and reservoir pressure state (each column). Photos a, b, c, etc. correspond to experiments 1, 2, 3, etc. unless otherwise noted; for parameters, see Table 1. For scale, the reservoir in all photos is 10 (+/− 2) cm in diameter. We label the horizontal and vertical positions as x and z. Black dashed lines outline the dikes and black arrows show their movement. Photo (a) shows an example from reservoir setup 2 (see section 2.1) while the others show setup 1. (a and b) Hoop stresses around the reservoir (shown by white dashed lines) encourage or inhibit dike opening, causing the dike to propagate laterally. (c and d) Experiment 3, overpressurized and then underpressurized. Dikes change orientation to open against σ_3, and the preferred path is traced by the dashed white lines. (e and f) Two views are presented to have a sense of the 3-D geometry of oblique dikes. The stars indicate contact between the dike and balloon. The dikes rotate horizontally and vertically into their preferred orientations. (g) The overpressure scenario is omitted, since the dike would go straight into the reservoir. The dike initially curls into a concentric shell, but the driving pressure forces it to escape this path.

1; Figure 3a), the hoop stresses were extensional, which helped the dike propagate toward the reservoir, while the reverse occurred for the underpressurized experiment (experiment 2; Figure 3b). In the underpressure experiment, the dike propagated horizontally away from the reservoir upon encountering its stress field. After the dike passed around the stress field, it resumed vertical propagation.

Experiment 1 was set up in a way that allowed us to assess how liquid exchange occurred between the dike and reservoir. We observed that the dike intersected with the reservoir and that the two immiscible fluids stratified due to density contrast. The dike allowed a relief of pressure in the reservoir (observed using polarized film) and afterward continued propagating vertically toward the surface. We do not have pressure data for the dike to be able to quantify our results, but we do discuss these observations later in section 4.

Other experiments, with nonradial dikes, had a second class of response, in which dikes curled and twisted into new orientations (Figures 3c–3g). They reoriented according to σ_3, so for overpressurized experiments (experiments 3 and 5; Figures 3c and 3e), the dikes curled inward to propagate toward the reservoir. For underpressurized experiments (experiments 4, 6, and 7; Figures 3d, 3f, and 3g), σ_3 is radial to the reservoir, so the dike reoriented to propagate tangentially around it. After these dikes passed around the reservoir, they began to escape its stress field, and their paths transitioned from curved to linear. As a result, they never formed perfect shells around the reservoir; instead, they took more of a tulip-flower-petal like shape. Both oblique and coaxial dikes changed orientation to become circumferential dikes.

In addition to these two classifications of dike response, we noticed that dikes generally propagate either toward or away from the reservoir, depending on the reservoir's pressure state (i.e., overpressurized or underpressurized). Overpressurized reservoirs tend to attract dike, either due to hoop stresses or σ_3 orientation, and in each case the dike intersected with the reservoir. Conversely, underpressurized reservoirs prevented dikes from approaching the reservoir, and in each case the dike was forced horizontally away, to then erupt at the surface.

3.2. Quantifying Dike Response

We characterize dike response via visual analysis. As noted, radial dikes responded by propagating laterally, while other, nonradial dikes responded by changing orientations. We analyze these two responses separately. For experiments with nonradial dikes (experiments 3–7), only a single photo taken at the end was necessary to quantify the results, since the shape of the dike records its history of interaction with the stress field (Figure 4a). We traced its shape in an illustration software to assist with detection of the dike, which sometimes was obscured by features that would hinder automated dike tracking (e.g., polarized light fringes; dike overlapping the reservoir). We processed the output in Matlab to measure the dike's position as a function of depth, relative to the balloon reservoir (Figure 4b). These dikes respond to reservoir stress by changing orientation, so we analyze the magnitude of orientation change as a proxy for dike response (Figure 4c), using the parameter $\partial^2 x/\partial z^2$, where x and z are, respectively, the horizontal and vertical components of the dike's position. In short, we quantify the location of each pixel in a photo of the dike and see how it compares with its neighboring pixels.

For dikes with initially strike-radial orientations, we note that two locations on the dike are important to describe how the dikes behaved: the point nearest to the reservoir and a point that indicates where the dike fractured the medium and grows the crack's surface as it propagates (Figure 4d). We used each frame of a time lapse to determine the location of the nearest point on the dike to the reservoir and pairs of sequential frames to determine where the dike was in the process of fracturation. We analyzed these frame pairs in Matlab, and, by taking the difference between the two, we could highlight this crescent-shaped new surface (Figure 4e). We calculated the geometric center to represent this area and track how it moves horizontally due to the reservoir's stress field, which we quantify using the parameter $\partial x/\partial z$ (Figure 4f).

To be able to compare our experiments with nature, we first normalize the radius, r; the x and z components of the radius; and the dike breadth, B, by the reservoir radius, r_{res}, into dimensionless forms, respectively, r^*, x^*, z^*, B^*:

$$r^* = r/r_{res}, \tag{12}$$

$$x^* = x/r_{res}, \tag{13}$$

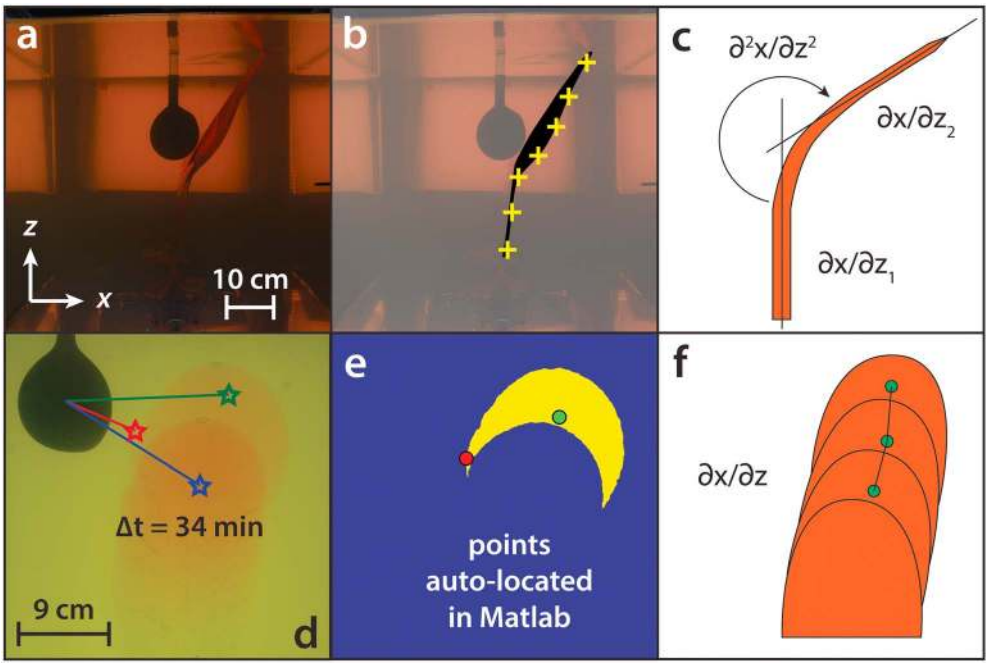

Figure 4. (a) In some experiments, the dike was not easy to see (experiment 7). (b) In such cases, we manually traced the dike in an illustrating software (black region), which helped us to quantify its path in Matlab (yellow + signs). For dikes that were distinct from the background, we did no manual tracing. (c) For nonradial dikes, the response is quantified by how abruptly it changes orientation, via the parameter $\partial^2 x/\partial z^2$. (d) Sequential photos (overlapped) of a propagating dike (experiment 2). Two important points on the dike: that nearest to the reservoir center (red star) and the geometric center of where fracturation is occurring between sequential frames (marked by the green star). Also included is the center of the roughly penny-shaped head region of the dike (blue star). (e) In Matlab, subtracting one photo from the next in a sequence highlights the differences between the two and illustrates where the dike was growing. The "two important points" are automatically located (green/red dots). (f) We analyze strike-radial dikes by tracking their change of horizontal position, represented by $\partial x/\partial z$.

$$z^* = z/r_{res}, \tag{14}$$

$$B^* = B/r_{res}. \tag{15}$$

We similarly use the dimensionless form of the dike response parameters, so instead of $\partial^2 x/\partial z^2$, we use $\partial^2 x^*/\partial z^{*2}$; $\partial x/\partial z$ is inherently dimensionless.

As nonradial dikes ascend from below, they change orientation as a function of σ^* (introduced in section 2.2). In the case of overpressurized experiments, this is a straightforward, power law relationship. In the case of underpressurized reservoirs, when these dikes bypass the reservoir, they leave its stress field and transition from curved to linear trajectory. When this occurs, the change of orientation response, $\partial^2 x^*/\partial z^{*2}$, drops. The relationship between σ^* and $\partial^2 x^*/\partial z^{*2}$ for a dike entering the stress field is different from the relationship for one leaving the stress field. We therefore analyze data for the first relationship only, to be able to compare with overpressurized experiments and to be able to characterize where a dike "feels" the stress due to the reservoir. All nonradial experiments are plotted together (Figure 5a) and form a common power law trend:

$$\partial^2 x^*/\partial z^{*2} = 61.4\sigma^{*2.4}. \tag{16}$$

For the strike-radial dikes, we performed a similar analysis. These dikes remained vertically oriented and preferred to rise vertically, due to their buoyancy. They only deviated from vertical propagation because of the stress field due to the reservoir (Figures 3a and 3b), as hoop stresses close to the reservoir are relatively high. In the underpressurized experiments, the dike eventually passed around the stress field and continued to propagate vertically. Similar to nonradial dikes, we analyzed the response as the dike entered the stress field to compare the two experiments and quantify where the dike begins to "feel" the stress due to the

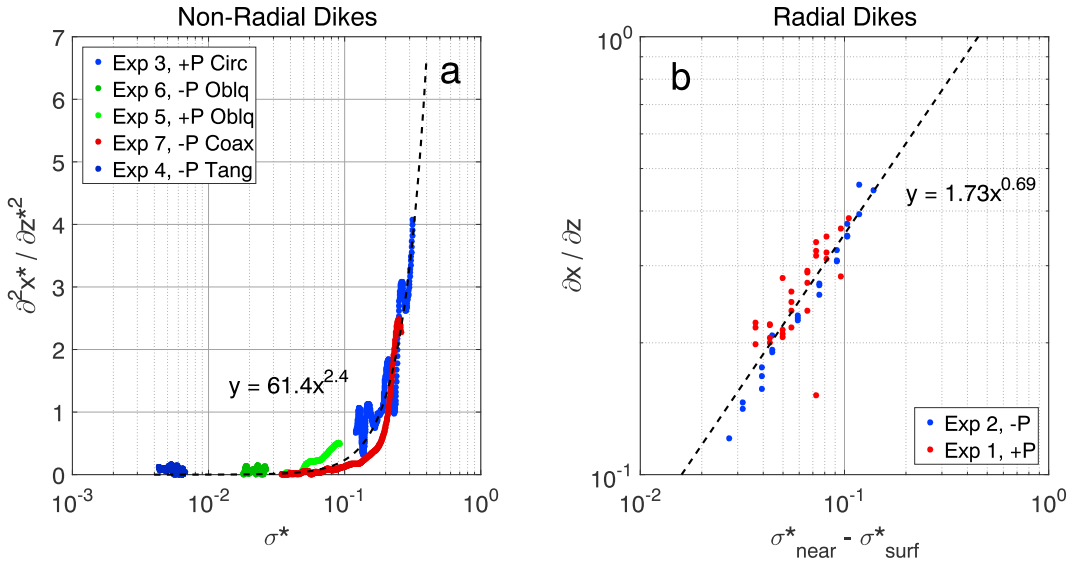

Figure 5. (a) Results from the nonradial dikes. The rate at which the dike changes orientation, $\partial^2 x^*/\partial z^{*2}$, is a function of dimensionless stress, σ^*. We show this as a semi log plot since some points are a bit less than zero on the vertical axis. We include a best-fitting power law curve (black, dashed line). (b) The stress difference between two points on a dike, σ^*_{near}–σ^*_{frac}, form a relationship with the degree to which it deflects horizontally, $\partial x/\partial z$. We again plot a best-fitting curve.

reservoir. As noted, we found that the dike's response, $\partial x/\partial z$, is a function of the stress at two points on the dike's surface: its nearest point to the reservoir, σ^*_{near} (Figure 4d, red star), and the geometric center of where fracturation is occurring, σ^*_{frac} (Figure 4d, green star). When we view its behavior against the difference in stress between these two points, a power law relationship emerges (Figure 5b):

$$\partial x/\partial z = 1.73\left(\sigma^*_{\text{near}} - \sigma^*_{\text{frac}}\right)^{0.69}. \tag{17}$$

3.3. Quantifying the Effective Radius of Interaction

At this moment, we can describe the degree to which a dike deflects as a function of the stresses in the crust. Dikes that feel very little stress deflect to a very small degree. We want to understand how close a dike needs to be to a reservoir before it is significantly affected by the stress field and the radius at which this occurs we define as a critical radius, r^*_{crit}.

3.3.1. Nonradial Dikes

For circumferential, oblique, and coaxial orientations, dikes respond to the medium stresses by changing orientation, which becomes pronounced as they approach σ^* of 0.1 (Figure 5a). We define this value as a critical stress, σ^*_{crit}, and it tells the location of r^*_{crit}. For σ^* at the reservoir's wall, ΔP^*, we use equations (3), (5), and (12) to derive:

$$r^*_{crit} \sim \left(\Delta P^*/\sigma^*_{crit}\right)^{1/3}. \tag{18}$$

For $\sigma^*_{crit} = 0.1$, the critical radius is therefore a function of only ΔP^*. In section 4.1, we will convert these dimensionless findings into plausible values for nature.

3.3.2. Radial Dikes

We perform a similar analysis to scale up the results from the radially oriented dikes (Figures 3a and 3b). In section 3.2, we noted that the degree to which a dike is horizontally deflected depends on the stress difference between nearest point on the dike (Figure 4d, red star) and a point at the geometric center of newly created surface (Figure 4d, green star). For a dike whose center (Figure 4d, blue star) is located at x_{cent} and z_{cent}, assuming a penny-shaped crack, the dimensionless stress of the nearest point, σ^*_{near}, is

$$\sigma^*_{near} = \Delta P^*/\left[r^*(x_{cent}, z_{cent}) - B^*/2\right]^3. \tag{19}$$

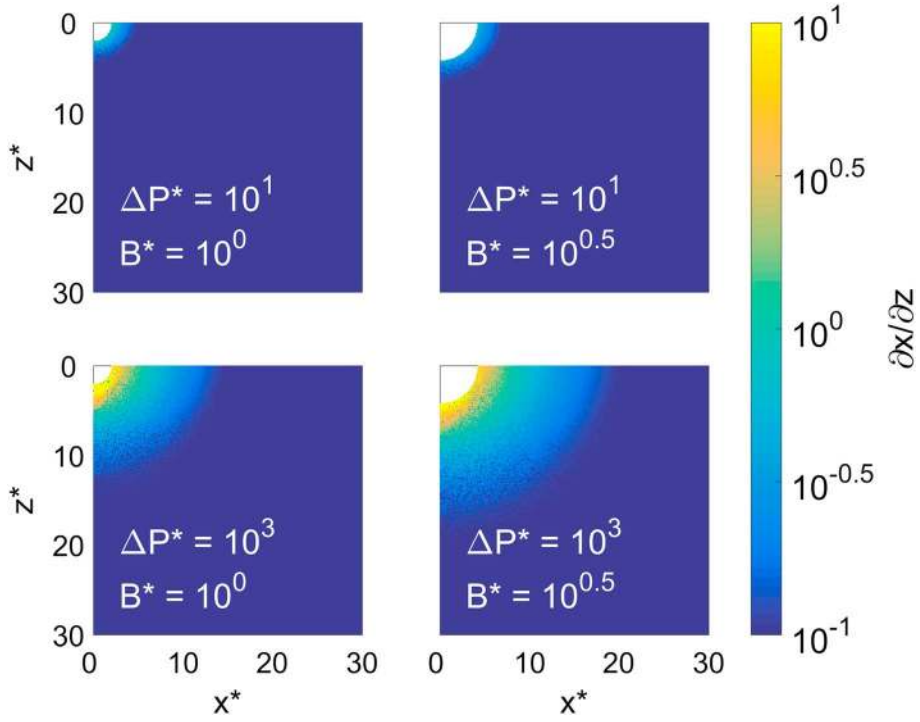

Figure 6. Maps of $\partial x/\partial z$ (color bar) for different dimensionless dike sizes, B^*, and dimensionless reservoir pressures, ΔP^*. These are generated numerically using Matlab, by finding the location of x_{frac} and z_{frac} that allows equations (17) and (21) to be equal, for any location of the dike center, then displaying the corresponding value of $\partial x/\partial z$. We define that the dike begins to respond where $\partial x/\partial z > 10^{-1}$ (which we set as the lower limit of the color bar). The horizontal and vertical axes are dimensionless positions with the reservoir center at (0,0). The white region in the upper, left corner represents the locations where the dike touches the reservoir and is therefore larger for large-breadth dikes (right column). Deflection is larger at higher pressures (bottom row).

The geometric center of where fracturation is occurring, located at x_{frac} and z_{frac}, does not have a set location; we only know that it is somewhere on the dike. However, we can easily calculate the stress, σ^*_{frac}, for any point on the dike:

$$\sigma^*_{frac} = \Delta P^* / r^*\left(x_{frac}, z_{frac}\right)^3. \tag{20}$$

With σ^*_{near} and σ^*_{frac}, we can estimate $\partial x/\partial z$ at any point, via equation (17). The deflection of the dike is also defined as the degree to which the center of the crack moves horizontally as it ascends:

$$\partial x/\partial z = \left(x_{frac} - x_{cent}\right)/\left(z_{frac} - z_{cent}\right). \tag{21}$$

When combining equations (17), (18), (20), and (21), no analytical solution can be derived for the location of x_{frac} and z_{frac}. Instead, we numerically model its location in Matlab by finding the point which best allows equations (17) and (21) to be equal, for a corresponding initial location of the dike center (Figure 4d, blue star), as function of ΔP^* and B^* (some solutions are shown in Figure 6). In this way, for any point at x_{cent} and z_{cent}, we locate the point at x_{frac} and z_{frac}, estimate σ^*_{near} and σ^*_{frac}, via equations (19) and (20), and finally estimate $\partial x/\partial z$ using either equations (17) or (21). This methodology allows us to map out $\partial x/\partial z$ for any ΔP^* and B^* (Figure 6). It is worth noting that in the negative ΔP case, x_{frac} is further away than x_{cent}, since dikes deflect away from the reservoir, while the reverse is true for positive ΔP; even so, the stress difference tends to be dominated by σ^*_{near}, so the $\partial x/\partial z$ maps for both $-\Delta P$ and $+\Delta P$ look similar.

To find the r^*_{crit} for these radial dikes, we define a critical deflection at $\partial x/\partial z = 0.1$, in which the dike deflects horizontally 1 m for every 10 m it ascends; we choose this value since it is at the lower limit of our experimental observations (Figure 5b). The ΔP^* and B^* parameters affect r^*_{crit}, so we attempt to define an

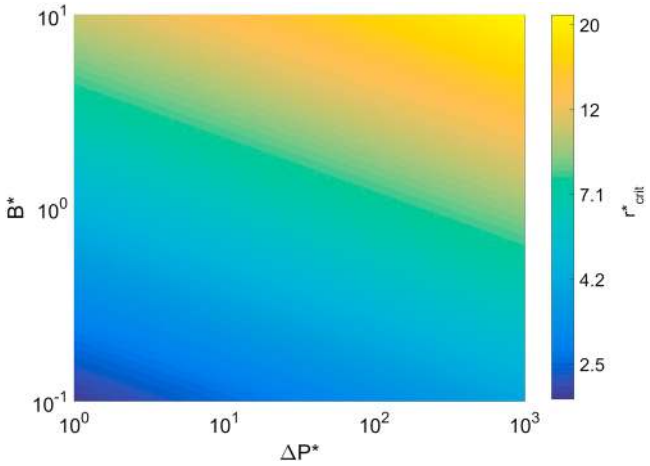

Figure 7. A surface showing at what distance strike-radial dikes begin to respond, r^*_{crit} (color bar), against dike size, B^*, and reservoir pressure, ΔP^*. Overpressure and underpressure conditions yield similar r^*_{crit}.

empirical relationship between the three, so that we can know if the dike is within the r^*_{crit}, without having to consider its nearest point or the geometric center of new surface creation. We consider B^* on the range of 10^{-1}–10^{1}, to analyze dikes much smaller and much bigger than the reservoir. They follow a power law, such that $r^*_{crit} = a\sigma^{*b}B^{*c}$, so we find a best-fitting surface, for the variables a, b, and c, which allows us to make an estimate of critical radius for a range of pressures and dike size (Figure 7). We will scale this information to natural systems in the next section.

$$r^*_{crit} = 2.87\Delta P^{*0.24}B^{*0.15}. \quad (22)$$

4. Discussion

4.1. Dimensions of the Critical Radius

We scale the dimensionless results presented above for plausible natural conditions, using equations (18) and (23), respectively, for nonradial and radial dikes. For these equations, r^*_{crit} can be described as functions of ΔP^* and B^*. We performed an analysis for $10^0 < \Delta P^* < 10^3$, which correspond to ΔP of 10^5–10^8 Pa, assuming values of E and $\Delta\rho$ listed in Table 2 and therefore a fracture pressure magnitude of 10^5 Pa. The parameters r^*_{crit} and B^* are proportional to the reservoir's radius and can be easily converted back to dimensions via equations (12) and (15). In this example we consider the dike's horizontal breadth to be 1 or 10 km. We therefore view the critical radius against reservoir radius; reservoir pressure; and, for radial dikes, dike breadth (Figure 8). For example, a 1-km radius reservoir will likely affect dikes within a 2- to 20-km radius, depending on the reservoir pressure, numbers on the same order of magnitude as previous numerical models (Karlstrom et al., 2009).

4.2. Spherical Nature of the Reservoir

We model the magma storage region as a spherical reservoir because it is practical to construct in the lab using a balloon and, although the balloon reservoir in our experiments did not always deform perfectly

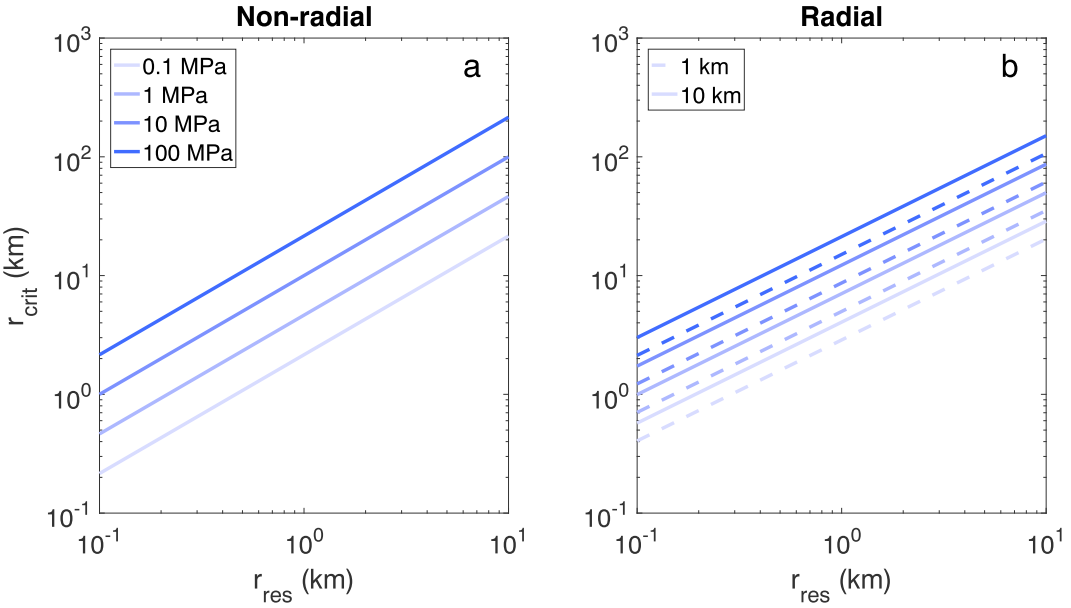

Figure 8. We estimate the radius, r_{crit}, at which dikes begin to deflect, for varying reservoir radius, r_{res}, and pressure (color shading) at natural scale. (a) For non-radial dikes, estimated via equation (18). Line shading represents estimates for different reservoir pressures. (b) For radial dikes via equation (23). Shadings and pressures are as in (a). Dashed and solid lines represent horizontal dike breadths of 1 and 10 km, respectively.

uniformly (probably due to heterogeneous strength of the balloon material; see Figure 3b), it models a simple, spherical (or nearly spherical) stress field. It should be noted, however, that the shape of the reservoir controls the shape of the surrounding stress field and, in turn, how dikes will propagate in its vicinity.

Unfortunately, we arrive to the problem that no one really knows the geometry of an active magma storage region. Field evidence of extinct systems indicates that intrusive bodies are built incrementally by layering of sills (Barnett & Gudmundsson, 2014; Menand, 2011; Menand et al., 2010). Ground deformation data, however, imply that reservoirs commonly undergo inflation when pressurized, which at the surface can be modeled as a point expansion (Pascal et al., 2014). Whether the actual form of a reservoir is roughly elliptical or is a stack of hydraulically connected sills and dikes remains open to debate. Gudmundsson (2012) points out that elliptical reservoirs are thermally stable, while protrusions (dikes and sills) extending from such a body are prone to solidification. We feel that a hydraulically connected network of dikes and sills, when pressurized, may exert a stress field on the crust that at a distance, can be approximated to a point expansion. At any rate, the stresses due to inflation are evident on the earth's surface, so we can be sure that they exist elsewhere in the crust as well and that dikes will be encouraged to deflect wherever they are present.

It is likely that aspect ratio of a natural magmatic reservoir dictates the degree to which our findings are applicable. Highly elongated (e.g., very flat, very tall, and narrow) reservoirs will generate a stress field that is fundamentally different to what we model, and dikes would therefore have a different response from what we observed. We expect low to moderate aspect ratio reservoirs to affect dikes in a similar fashion to our study. Moderately oblate ellipses concentrate stress on their out horizontal margins (Gudmundsson, 2006, 2012), which should affect dike further away than a spherical geometry. Conversely, prolate ellipsoids concentrate stress on the vertical margins of the reservoir, meaning dikes would be affect only when nearer.

4.3. Relation to Various Volcanic Behavior

4.3.1. Reservoir-Avoiding Dikes

Our findings that dikes can propagate around a reservoir (Figures 3d and 3f) relate to some observations made in nature. Anderson (1937) documented outward-dipping, circumferential dikes at Ardnamurchan dike swarm and hypothesized their orientation was due to an underpressurized reservoir, though he modeled the dikes as originating from the reservoir (ring dikes), rather than below. Magee et al. (2012) proposed that those dikes indeed flowed around the reservoir (albeit laterally), supplied from regional dikes. At the Mt. Somma scarp (next to Vesuvius), Porreca et al. (2006) made similar observations of dikes that have a variety of orientations, ranging from circumferential to oblique to radial, and determine that these orientations may have been a result of the reservoir pressure (overpressured or underpressured) at the time of emplacement. In either example, we would expect a dike originating from below the reservoir (passing around it) to be mafic in composition. This seems to be the case at the Mt. Somma scarp, in which exposed dikes and lavas are more mafic than many of the other products (both plinian and interplinian) in the locality (Ayuso et al., 1998).

4.3.2. Eruptive Cycles

We can continue to consider the effects of underpressure reservoirs in the context of observations made by Takada (1997), who documents a cyclic pattern at several volcanoes, including Fuji, Etna, and Mauna Loa. Takada finds that flank vents following a major eruption tend to be located far away from the central vent and that subsequent events become progressively nearer as the central edifice approaches another period of activity, which occurs on a time frame of 400–1,000 years. An eruption deflates the reservoir to some degree and places the surrounding crust in a state of extension, which inhibits dike propagation close to the reservoir. In this case, an ascending dike will likely be deflected away from the volcanic center and could then erupt as a flank eruption (Figure 9). Further eruptions sourced from the reservoir would be unlikely until either the stresses in the crust relaxed, thus allowing dikes to penetrate the magma storage region, or magma somehow managed to enter the reservoir and repressurize it (i.e., magma supplied to the reservoir by a stable, long-lived conduit). As the reservoir repressurizes, the extensional stresses weaken, and the deflection of dikes becomes less pronounced. This pattern of behavior is difficult to explain by assuming the dikes are sourced from an overpressurized reservoir. After a major eruption, a volcano would not have the high internal pressure necessary to drive a dike far away.

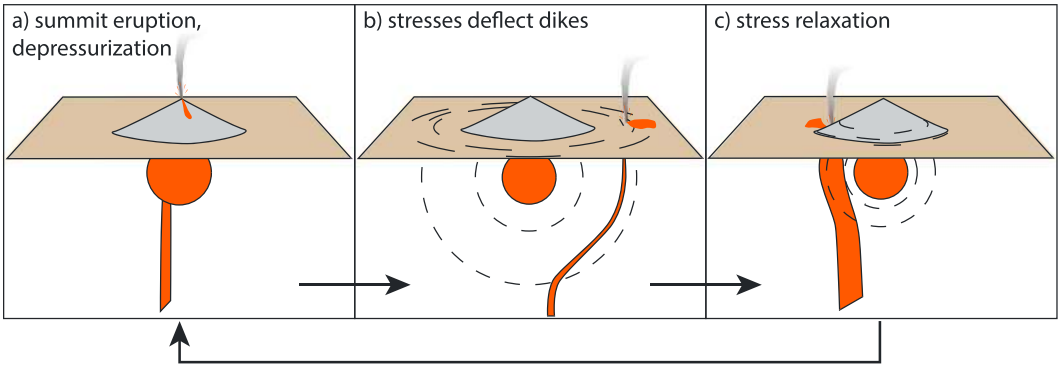

Figure 9. Proposed mechanism for the cyclic pattern of flank eruptions, driven by reservoir depressurization. Summit eruptions depressurize the reservoir and place the crust in a state of extension, which deflects dikes away. As the stress decreases, either due to repressurization or stress relaxation, the deflection becomes less pronounced. Eventually, dikes are no longer deflected and the cycle can repeat.

If we assume the crust behaves like a Maxwell material, the stress surrounding the reservoir relaxes with time, t, such that

$$\sigma(t) = 2\,G\,\varepsilon_0\ \exp(-G\,t/\eta) = [\Delta P/(1+\nu)]\ \exp(-G\,t/\eta), \tag{23}$$

where ε_0 is the initial strain and G and η are the crust's shear modulus and viscosity (Segall, 2010). This assumes the initial strain is linearly related to the reservoir pressure, $\varepsilon_0 \approx \Delta P/E$, since the material behaves elastically on this short initial timescale, and that $G = E/2(1+\nu)$. Using equations (18) and (23), we estimate the r^*_{crit} as a function of time and the initial pressure (Figure 10), for values of $\eta = 1{,}020$ Pa/s (Di Giuseppe et al., 2009) and $G = 30$ GPa. The initial magnitude of r^*_{crit} depends strongly on the initial pressure, but the long-term value of r^*_{crit} becomes small on the order of 100 years for any initial pressure. This has some agreement with Takada's (1997) findings, in which dikes cycle through this relaxation/pressurization pattern on the order of hundreds to 1,000 years.

4.3.3. Eruption Triggering

An important observation from our experiments is that dikes that breach a magmatic reservoir do not necessarily cease propagation (Figures 11a and 11b). In experiment 1, the dike was attracted to the overpressurized reservoir, and, after it made contact, the dike continued to propagate. In our experiment, the two immiscible liquids stratified by density and the reservoir liquid (neutrally buoyant in gelatin) provided no buoyant force to continue propagation; therefore, propagation was driven by buoyancy of the oil (the liquid filling the dike) and by the slight overpressure of the reservoir. In a natural analogue, the magma in a reservoir would be equally or more buoyant than the magma in a mafic dike. It could therefore flow inside of the dike and take advantage of the existing fracture to propagate toward the surface (Figure 11c).

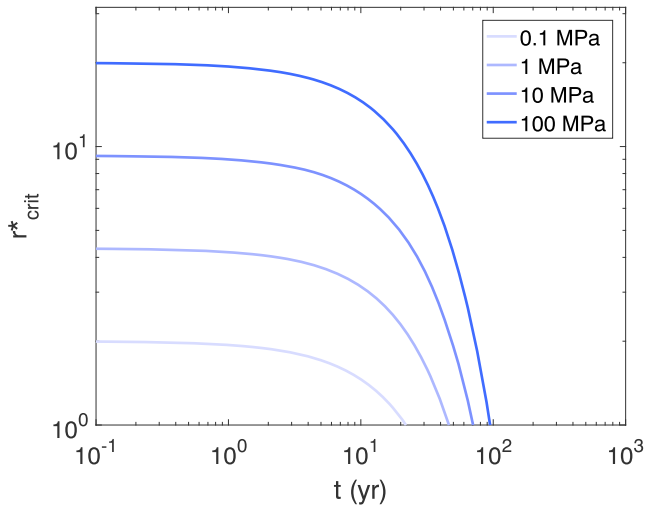

Figure 10. Time evolution of the critical radius of nonradial dike deflection due to viscoelastic relaxation. Shading represents different initial magnitudes of reservoir pressure. The initial stress relaxes with time, so the critical radius diminishes.

This has implications for eruption triggering, in that a basaltic dike may help to open a pathway along which more-evolved magmas from a shallow reservoir can migrate. Takeuchi (2004) shows that some cataclysmic eruptions of very viscous magma were preceded by precursory eruptions of magma generally a few orders of magnitude less viscous. It is conceivable that such eruptions are initiated by deeply sourced basaltic dikes which, upon breaching the reservoir, encourage eruption via a combination of mechanisms: (1) remobilization of the residing magma (Murphy et al., 2000; Ruth et al., 2016); (2) providing a low-viscosity lubricating layer inside of the dike, which the viscous evolved magma slides along (Watts et al., 1999); (3) providing a large fracture, which requires less pressure to open widely than a small fracture (Rubin, 1995).

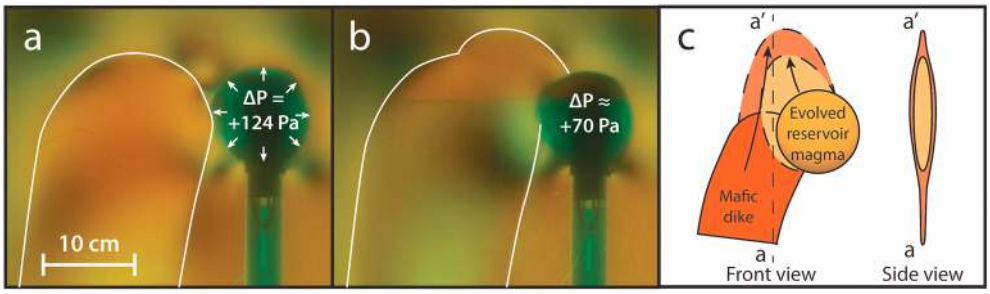

Figure 11. (a and b) An example from experiment 1 (cross-sectional view), showing that dike propagation may continue after a dike intersects a reservoir. (c) A model for the extraction of viscous reservoir magma into a basaltic dike. The basalt lubricates and propagates the fracture, while the overpressure and buoyancy of the reservoir magma open the fracture wide.

4.4. Driving Pressure

We note that our results have been influenced to some degree by the dikes' driving pressures, which is especially obvious in experiment 7 (Figure 3g). Dikes with a significant internal pressure seem to propagate according to their own internally derived local stress field (i.e., they propagate along a straight path) and only alter course when affected by a significant external stress (e.g., reservoir stresses and regional stresses). As they escape the external stress field, they continue propagating straight. This behavior is also exhibited to a lesser degree for other experiments that had an underpressurized reservoir. It seems that this balance between internal and external pressure sources may dictate the degree to which a dike deviates from its quasi-static path. We account for this to some degree in our scaling of experiments, in that σ^* is scaled by the dike's fracturation pressure (which itself is a function of buoyancy and the Young's modulus); however, the internal pressure can be much higher than the fracturation pressure, which is likely the case in a constant-flux experiment (experiment 7). Constant-volume experiments should have an internal pressure close to the fracturation pressure.

5. Conclusions

We present an investigation on how dikes respond to the stress field around a pressurized magma storage region and found two classifications of response. Nonradial dikes reorient to open against σ_3 and therefore propagate either radially or tangentially to an overpressurized or underpressurized reservoir, respectively. Radial dikes do not change orientation, but rather propagate laterally at their fringes due to the hoop stresses around the reservoir. Overpressurized reservoirs generate extensional hoop stresses, which help a dike to propagate toward the reservoir, while the reverse occurs for an underpressurized reservoir.

These two classes of interaction behave as functions of the stress distribution due to the reservoir and, in both cases, the higher the stress, the more pronounced the reaction. For nonradial dikes, it is a function of the stress at the dike's vertical leading tip. For radial dikes, the stress has a more complex role, and we find that lateral propagation functions according to the stress difference between two points: the point nearest to the reservoir and a point at the center of where fracturation is occurring as it propagates.

Dikes that ascend near a reservoir are likely to cause volcanic crises, regardless of the state of pressure. By quantifying a volcano's reservoir pressure, however, we can anticipate whether dike will propagate toward or away from it and therefore whether it is likely to cause an eruption near to, or far from, the central vent, information that is vital for hazards management purposes. The degree to which we accurately estimate competing stress sources, that is, the driving pressure of a dike, the local stresses due to the reservoir and broader regional stresses, will dictate our ability forecast where dikes are likely to erupt.

Acknowledgments
This work comprises Earth Observatory of Singapore contribution no. 222. This research is supported by the National Research Foundation Singapore (award NRF2015-NRF-ISF001-2437) and the Singapore Ministry of Education under the Research Centres of Excellence initiative. It has also been partly funded by the Dr. Stephen Riady Geoscience Scholars Fund. Our data are available at https://doi.org/10.26074/5zwv-7j56. This is under DR-NTU, a local instance of Dataverse, supported by Nanyang Technological University. For more information, please see the supporting information.

References

Anderson, E. M. (1937). IX.—The dynamics of the formation of cone-sheets, ring-dykes, and caldron-subsidences. *Proceedings. Royal Society of Edinburgh*, *56*, 128–157. https://doi.org/10.1017/S0370164600014954

Ayuso, R. A., De Vivo, B., Rolandi, G., Seal, R. R., & Paone, A. (1998). Geochemical and isotopic (Nd-Pb-Sr-O) variations bearing on the genesis of volcanic rocks from Vesuvius, Italy. *Journal of Volcanology and Geothermal Research*, *82*(1-4), 53–78. https://doi.org/10.1016/S0377-0273(97)00057-7

Bagnardi, M., Amelung, F., & Poland, M. (2013). A new model for the growth of basaltic shields based on deformation of Fernandina volcano, Galápagos Islands. *Earth and Planetary Science Letters*, *377-378*, 358–366. https://doi.org/10.1016/j.epsl.2013.07.016

Barnett, Z. A., & Gudmundsson, A. (2014). Numerical modelling of dykes deflected into sills to form a magma chamber. *Journal of Volcanology and Geothermal Research*, *281*, 1–11. https://doi.org/10.1016/j.jvolgeores.2014.05.018

Bianco, F., Castellano, M., Milan, G., Ventura, G., & Vilardo, G. (1998). The Somma-Vesuvius stress field induced by regional tectonics: Evidences from seismological and mesostructural data. *Journal of Volcanology and Geothermal Research*, *82*(1-4), 199–218. https://doi.org/10.1016/S0377-0273(97)00065-6

Chadwick, W. W. Jr., & Dieterich, J. H. (1995). Mechanical modeling of circumferential and radial dike intrusion on Galapagos volcanoes. *Journal of Volcanology and Geothermal Research*, *66*(1-4), 37–52. https://doi.org/10.1016/0377-0273(94)00060-T

Corbi, F., Rivalta, E., Pinel, V., Maccaferri, F., & Acocella, V. (2016). Understanding the link between circumferential dikes and eruptive fissures around calderas based on numerical and analog models. *Geophysical Research Letters*, *43*, 6212–6219. https://doi.org/10.1002/2016GL068721

Crabtree, S. M., & Waters, L. E. (2017). The petrologic history of the Sanganguey volcanic field, Nayarit, Mexico: Comparisons in a suite of crystal-rich and crystal-poor lavas. *Journal of Volcanology and Geothermal Research*, *336*, 51–67. https://doi.org/10.1016/j.volgeores.2017.02.005

Daniels, K. A., & Menand, T. (2015). An experimental investigation of dyke injection under regional extensional stresses. *Journal of Geophysical Research: Solid Earth*, *120*, 2014–2035. https://doi.org/10.1002/2014JB011627

Delaney, P. (1986). Field relations between dikes and joints: Emplacement processes and paleostress analysis. *Journal of Geophysical Research*, *91*(B5), 4920–4938. https://doi.org/10.1029/JB091iB05p04920

Di Giuseppe, E., Funiciello, F., Corbi, F., Ranalli, G., & Mojoli, G. (2009). Gelatin as rock analogs: A systematic study of their rheological and physical properties. *Tectonophysics*, *473*(3-4), 391–403. https://doi.org/10.1016/j.tecto.2009.03.012

Galland, O., Burchardt, S., Hallot, E., Mourgues, R., & Bulois, C. (2014). Dynamics of dikes versus cone sheets in volcanic systems. *Journal of Geophysical Research: Solid Earth*, *119*, 6178–6192. https://doi.org/10.1002/2014JB011059

Galland, O., Holohan, E., van Wyk de Vries, B., & Burchard, S. (2015). Laboratory modelling of volcano plumbing systems: A review. In *Advances in volcanology* (pp. 1–68). Berlin, Heidelberg: Springer. https://doi.org/10.1007/11157_2015_9

Gudmundsson, A. (2006). How local stresses control magma-chamber ruptures, dyke injections, and eruptions in composite volcanoes. *Earth Science Reviews*, *79*(1-2), 1–31. https://doi.org/10.1016/j.earscirev.2006.06.006

Gudmundsson, A. (2012). Magma chambers: Formation local stresses, excess pressures, and compartments. *Journal of Volcanology and Geothermal Research*, *237-238*, 19–41. https://doi.org/10.1016/j.jvolgeores.2012.05.015

Gudmundsson, A., Lecoeur, N., Mohajeri, N., & Thordarson, T. (2014). Dike emplacement at Bardarbunga, Iceland, induces unusual stress changes, caldera formation, and earthquakes. *Bulletin of Volcanology*, *76*(10), 869. https://doi.org/10.1007/s00445-014-0869-8

Karlstrom, L., Dufek, J., & Manga, M. (2009). Organization of volcanic plumbing through magmatic lensing by magma chambers and volcanic loads. *Journal of Geophysical Research*, *114*, B10204. https://doi.org/10.1029/2009JB006339

Kavanagh, J.,. L., Boutelier, D., & Cruden, A. R. (2015). The mechanics of sill inception, propagation and growth: Experimental evidence for rapid reduction in magmatic overpressure. *Earth and Planetary Science Letters*, *421*, 117–128. https://doi.org/10.1016/j.epsl.2015.03.038

Kavanagh, J.,. L., Menand, T., & Daniels, K.,. A. (2013). Gelatin as a crustal analogue: Determining elastic properties for modelling magmatic intrusions. *Tectonophysics*, *582*, 101–111. https://doi.org/10.1016/j.tecto.2012.09.032

Lee, B. J., Kee, S.-H., Oh, T., & Kim, Y.-Y. (2017). Evaluating the dynamic elastic modulus of concrete using shear-wave velocity measurements. *Advances in Materials Science and Engineering*, *2017*, 1651753. https://doi.org/10.1155/2017/1651753

Lister, J. R., & Kerr, C. (1991). Fluid-mechanical models of crack propagation and their application to magma transport in dykes. *Journal of Geophysical Research*, *96*(B6), 10,049–10,077. https://doi.org/10.1029/91JB00600

Maccaferri, F., Bonafede, M., & Rivalta, E. (2011). A quantitative study of the mechanisms governing dike propagation, dike arrest and sill formation. *Journal of Volcanology and Geothermal Research*, *208*(1-2), 39–50. https://doi.org/10.1016/j.jvolgeores.2011.09.001

Magee, C., Stevenson, C., O'Driscoll, B., Schofield, N., & McDermott, K. (2012). An alternative emplacement model for the classic Ardnamurchan cone sheet swarm, NW Scotland, involving lateral magma supply via regional dykes. *Journal of Structural Geology*, *43*, 73–91. https://doi.org/10.1016/j.jsg.2012.08.004

Menand, T. (2011). Physical controls and depth of emplacement of igneous bodies: A review. *Tectonophysics*, *500*(1-4), 11–19. https://doi.org/10.1016/j.tecto.2009.10.1016

Menand, T., Daniels, K. A., & Benghiat, P. (2010). Dyke propagation and sill formation in a compressive tectonic environment. *Journal of Geophysical Research*, *115*, B08201. https://doi.org/10.1029/2009JB006791

Menand, T., & Tait, S. (2002). The propagation of a buoyant liquid-filled fissure from a source under constant pressure: An experimental approach. *Journal of Geophysical Research*, *107*(B11), 2306. https://doi.org/10.1029/2001JB000589

Murphy, M. D., Sparks, R. S. J., Barclay, J., Carroll, M. R., & Brewer, T. S. (2000). Remobilization of andesite magma by intrusion of mafic magma at the Soufriere Hills volcano, Montserrat, West Indies. *Journal of Petrology*, *41*(1), 21–42. https://doi.org/10.1093/petrology/41.1.21

Nur Hanani, Z. A., Roos, Y. H., & Kerry, J. P. (2012). Use of beef, pork and fish gelatin sources in the manufacture of films and assessment of their composition and mechanical properties. *Food Hydrocolloids*, *29*(1), 144–151. https://doi.org/10.1016/j.foodhyd.2012.01.015

Pansino, S. & Taisne, B. (2018). Datasets relating to: How magmatic storage regions attract and repel propagating dikes. https://doi.org/10.26074/5zwv-7j56

Pascal, K., Neuberg, J., & Rivalta, E. (2014). On precisely modelling surface deformation due to interacting magma chambers and dykes. *Geophysical Journal International*, *196*(1), 253–278. https://doi.org/10.1093/gji/ggt343

Pinel, V., & Jaupart, C. (2003). Magma storage and horizontal dyke injection beneath a volcanic edifice. *Earth and Planetary Science Letters*, *221*(1-4), 245–262. https://doi.org/10.1016/S0012-821X(04)00076-7

Porreca, M., Acocella, V., Massimi, E., Mattei, M., Funciciello, R., & De Benedetti, A. A. (2006). Geometric and kinematic features of the dike complex at Mt. Somma, Vesuvio (Italy). *Earth and Planetary Science Letters*, *245*(1-2), 389–407. https://doi.org/10.1016/j.epsl.2006.02.027

Ramesh, K. (2000). *Digital photoelasticity—Advanced techniques and applications*. Berlin Heidelberg: Springer. https://doi.org/10.1007/978-3-642-59723-7

Rivalta, E., Böttinger, M., & Dahm, T. (2005). Buoyancy-driven fracture ascent: Experiments in layered gelatin. *Journal of Volcanology and Geothermal Research*, *144*(1-4), 273–285. https://doi.org/10.1016/j.jvolgeores.2004.11.030

Rivalta, E., Taisne, B., Bunger, A.,. P., & Katz, R.,. F. (2015). A review of mechanical model of dike propagation: Schools of thought, results and future directions. *Tectonophysics*, *638*, 1–42. https://doi.org/10.1016/j.tecto.2014.10.003

Rubin, A. M. (1995). Propagation of magma-filled cracks. *Annual Review of Earth and Planetary Sciences*, *23*(1), 287–336. https://doi.org/10.1146/annurev.ea.23.050195.001443

Ruth, D. C. S., Cottrell, E., Cortés, J. A., Kelley, K. A., & Calder, E. S. (2016). From passive degassing to violent strombolian: The case of the 2008 eruption of Llaima volcano, Chile. *Journal of Petrology*, *57*(9), 1833–1864. https://doi.org/10.1093/petrology/egw063

Schmiedel, T., Galland, O. & Breitkreuz, C. (2017). Dynamics of sill and laccolith emplacement in the brittle crust: Role of host rock strength and deformation mode.

Segall, P. (2010). *Earthquake and volcano deformation* (pp. 203–205). Princeton, NJ: Princeton University Press.

Taisne, B., & Tait, S. (2009). Eruption versus intrusion? Arrest of propagation of constant volume, buoyant, liquid-filled cracks in an elastic, brittle host. *Journal of Geophysical Research*, *114*, B06202. https://doi.org/10.1029/2009JB006297

Taisne, B., & Tait, S. (2011). Effect of solidification on a propagating dike. *Journal of Geophysical Research*, *116*, B01206. https://doi.org/10.1029/2009JB007058

Takada, A. (1997). Cyclic flank-vent and central-vent eruption patterns. *Bulletin of Volcanology*, *95*(B6), 8471–8556. https://doi.org/10.1029/JB095iB06p08471

Takeuchi, S. (2004). Precursory dike propagation control of viscous magma eruptions. *Geology*, *32*(11), 1001–1004. https://doi.org/10.1130/G20792.1

Tosh, S. M., Marangoni, A. G., Ross Hallett, F., & Britt, I. J. (2003). Aging dynamics in gelatin gel microstructure. *Food Hydrocolloids*, *17*, 503–513.

Urbani, S., Acocella, V., & Rivalta, E. (2018). What drives the lateral versus vertical propagation of dikes? Insights from analogue models. *Journal of Geophysical Research: Solid Earth*, *123*, 3680–3697. https://doi.org/10.1029/2017JB015376

Watanabe, T., Masuyama, T., Nagaoka, K., & Tahara, T. (2002). Analog experiments on magma-filled cracks: Competition between external stresses and internal pressure. *Earth, Planets and Space*, *54*(12), e1247–e1261. https://doi.org/10.1186/bf03352453

Watts, R. B., de Silva, S. L., Jimenez de Rios, G., & Croudace, I. (1999). Effusive eruption of viscous silicic magma triggered and driven by recharge: a case study of the Cerro Chascon-Runtu Jarita Dome Complex in Southwest Bolivia. *Bulletin of Volcanology*, *61*(4), 241–264. https://doi.org/10.1007/s004450050274